Gaze-Dependent Simulation of Light Perception in Virtual Reality

Laura R. Luidolt, Michael Wimmer, and Katharina Krösl

Fig. 1. Comparison of a standard renderer low light scene and our adaptations.

Abstract— The perception of light is inherently different inside a virtual reality (VR) or augmented reality (AR) simulation when compared to the real world. Conventional head-worn displays (HWDs) are not able to display the same high dynamic range of brightness and color as the human eye can perceive in the real world. To mimic the perception of real-world scenes in virtual scenes, it is crucial to reproduce the effects of incident light on the human visual system. In order to advance virtual simulations towards perceptual realism, we present an eye-tracked VR/AR simulation comprising effects for gaze-dependent temporal eye adaption, perceptual glare, visual acuity reduction, and scotopic color vision. Our simulation is based on medical expert knowledge and medical studies of the healthy human eye. We conducted the first user study comparing the perception of light in a real-world low-light scene to a VR simulation. Our results show that the proposed combination of simulated visual effects is well received by users and also indicate that an individual adaptation is necessary, because perception of light is highly subjective.

Index Terms—Perception, virtual reality, user studies

◆

1 INTRODUCTION

In this paper, we present a virtual reality (VR) and augmented reality (AR) simulation for the full light range perceivable by humans based on medical characteristics and perceptual evaluation. We combine effects for temporal eye adaptation, perceptual glare, reduction of visual acuity and scotopic color vision to recreate real-world light phenomena. Our simulation reacts to head motion, eye movements and changes in pupil size and runs in real time in VR. The results from our pilot user study show that we are able to simulate effects close to real-world experiences.

Many application areas, such as architectural planning, light planning, medical simulations or driving simulators, require photo-realistic computer simulations and, in case of VR applications, a high level of immersion. This includes detailed 3D models, accurate tracking, physically plausible lighting and a realistic simulation of perceptual effects produced by extreme lighting conditions, such as eye adaptation or glare.

Common low dynamic range (LDR) screens are only able to display a much smaller range of brightness than the range of light that is perceivable by the human visual system. Hence, these devices are

not able to represent extreme lighting conditions intrinsically, e.g., very bright light sources or a low-light ambiance. Furthermore, when looking at a desktop monitor, the ambient light of the surrounding environment influences the reaction of our pupils and the way our visual system processes the scene. Head-worn displays (HWDs) provide for a completely closed system, which allows us to control the amount of incident light reaching the eyes by avoiding any illumination from the physical environment.

Algorithms taking extreme lighting conditions or visual perception into account [18, 31, 45] were developed (and are still mainly used) for 2D displays. The perceptual differences of standard displays and HWDs are neglected. A user's light perception depends on many circumstances, for example, pupil size, visual acuity, or a person's age [12, 47], however, these factors are generally not accounted for. Current perceptual approaches that rely on the viewing direction are only focused on conventional 2D displays [24]. Moreover, 2D displays are not fully immersive. Thus, there is no need for the scene to be entirely perceptually correct, because the perception is not close to real life anyway.

VR HWDs, on the other hand, allow complete control of the human visual field, which is why we need methods especially designed for VR. Taking the viewing direction into account is also crucial since it determines how much light enters the eye. Therefore, accurate simulations need to react to eye-tracking data, which is not trivial for performance-intensive VR applications.

When attempting to create a realistic simulation of the human perception of light in VR, we face a number of challenges. First, the *displayable range* inside an HWD does not span the full range perceiv-

- *Laura R. Luidolt and Michael Wimmer are with TU Wien. E-mail: {luidolt | wimmer}@cg.tuwien.ac.at .*
- *Katharina Krösl is with VRVis Forschungs-GmbH. E-mail: kroesl@vrvis.at.*

able by a human. Therefore, we need a method to map the visible range to the small range of the display. Ordinary tone-mapping methods target the mapping of a high-dynamic range scene to the range of the output device. However, these operations do not consider extreme lighting conditions and their effects on the human visual system. Second, a VR display cannot exhibit the same *high intensities* as light sources in the real world. Hence, we cannot naturally experience blinding effects inside an HWD and need to simulate the glare that bright lights would create in the real world. Third, a VR display cannot represent *low-light* scenes accurately. The minimum displayable intensities of HWDs are still too high to invoke the range of scotopic vision for a user. Therefore, the color changes and reduced visual acuity we experience in real-world low-light scenes under scotopic vision need to be simulated artificially.

To overcome these challenges, we propose a simulation of human perception of light in VR, comprising effects for temporal eye adaptation, perceptual glare, reduced visual acuity and scotopic color vision, and incorporate eye tracking to allow for a gaze-dependent simulation.

We make the following contributions:

- We developed a **novel post-processing workflow** for more accurate light simulation in VR and AR, by combining and improving two state-of-the-art approaches [18,31] for a real-time application, running at 90 Hz and using live eye-tracking data. The presented method can be used for vision impairment studies [20], evaluating lighting conditions for architectural planning, as well as more realistic computer games.

- We simulate **temporal eye adaptation** using a Gaussian-weighted brightness value, centered around the gaze point, to reproduce the view-dependent influence of incident light. To replicate **reduced visual acuity**, as experienced in scotopic vision, we apply a Gaussian blur on the lightness values in CIE L*a*b* (Lab) color space, which is perceptually uniform and therefore more accurate than previous approaches [18]. We also include **scotopic color vision** in our simulation.

- We propose a **perceptual glare**, based on previous approaches using a point spread function (PSF) [17, 31] and informed by expert knowledge from an optometrist. By using an eye tracker, we are able to recalculate the glare kernel according to the user's live changes in pupil size and modify the intensity of the effect depending on the gaze direction of the user.

- We conducted the first **user study** that compares a real-world low-light situation to a VR simulation using a perceptual evaluation. Our results show that visual perception is different for each participant, yet overall, our simulation was able to give the impression of a realistic scene.

This paper is organized as follows: In Section 2 we explain the medical background details of the human eye and how we perceive light and color. Section 3 gives an overview over the current state of the art in related work. In Section 4 we lay out the methodology of this paper in detail and discuss the four main effects of human light perception and their application to a rendered image. We describe our conducted user study in Section 5 and present our results in Section 6. In Section 7 we discuss these results in detail and highlight benefits and limitations of our approach. Section 8 then concludes our work and Section 9 outlines possible directions for future work.

2 BACKGROUND

Many phenomena in human vision can be explained by considering the characteristics of the anatomy of the human eye, and the light incidence and processing.

It is commonly known that light has particle properties as well as wave properties. This is called the *light wave-particle-duality*, and light is the only known medium in which this phenomenon appears. In the remainder of this paper, we view the scattering of light on particles as a diffraction of waves on an obstacle.

The human eye is an ellipsoid with an average diameter of 24 mm along its longest axis and consist of multiple different tissues, which affect how we perceive light:

Cornea   Light entering the eye first hits the cornea. Irregularities in the surface structure can cause scattering errors [36]. When light rays deviate from their original path by less than $90°$, it is called *forward light scatter* (straylight). What we perceive as glare is forward-scattered light due to the eye's impurities and irregularities, mostly in the cornea and the lens. These small errors (further called particles) lead to common glare phenomena including a corona and a rainbow-colored halo.

Pupil   The pupil contracts and dilates from approximately 2 to 8 mm, responding to luminance changes of the viewed scene (*pupillary light reflex*) [29]. Retinal straylight depends on the pupil diameter [10]. The incidence of light through the pupil creates a so-called airy disk, which is defined by the wavelength of light and the aperture size [1].

Lens   The lens has a diameter of ~ 10 mm and focuses the incoming light rays on the retina [15]. In the lens cortex, protein structures, i.e., spherical particles, are arranged in a highly ordered alignment. Irregularities in this ordering or particles of increased size lead to interferences, which result in unevenly scattered light and, therefore, in retinal straylight [37]. In general, large particles, with a median radius of 724 nm, dominate the forward scattering [40].

Retina and Fovea   The retina converts the light that is projected onto it into a signal that is transmitted to the brain [15]. The fovea is a small area on the retina that has the highest concentration of photoreceptive cells and, therefore, is the point of sharpest vision. There are two types of photoreceptors in the retina, rods (~ 110–125 million) and cones (6.3–6.8 million) [15]. The cones are mainly located in the fovea and can be divided into three different types, which process long (~ 564 nm), medium (~ 534 nm) and short (~ 420 nm) wavelengths, for red, green and blue colors respectively, also called *photopic vision* [27]. Rods, on the other hand, are responsible for light and dark vision. Since there are no rods located in the fovea, we lose visual acuity at luminance levels where no cones are active ($< 0.03 \frac{cd}{m^2}$) and can only to discern shapes and movement in the dark – this is also called *scotopic vision*.

Colors in Scotopic Vision   During mesopic (i.e., between photopic and scotopic) and scotopic vision, the rods in the eye become more prominent than the cones, and a perceptual color shift towards green and blue colors occurs, called the *Purkinje effect*. The luminance sensitivity of photoreceptors in scotopic vision is the highest at approximately 507 nm, while the photopic sensitivity peaks at 555 nm [2].

Temporal Adaptation   Human perception also depends on the time spent under specific lighting conditions. For example, turning on a lamp in a dark room leads to oversaturation of the dark-adapted photoreceptors, and everything is too bright for a few moments, until we adapt to the new illumination. Dark to bright adaptation takes approximately 5 minutes [3], while it can take 20 to 30 minutes to adapt from bright sunlight to darkness.

3 STATE OF THE ART

Multiple related works aim to simulate displayed scenes more realistically and, therefore, rely on the medical basis of human vision.

3.1 Light Simulation Tools

Simulating light in a physically inspired and, therefore, perceptually pleasing way can be used in various applications. Meyer et al. [25] used perception-based methods to simulate glare situations at night-time on LDR displays for glares from oncoming vehicles' headlights. This research is merely targeted at 2D displays and does not include VR. Jones and Reinhart [16] proposed an application that predicts daylight glare probability and contrast in real time for architectural design. In contrast to this work, our simulation of human vision is able to run in real time in a VR application and therefore provides a higher level of immersion. Krösl et al. [19] simulated view-dependent eye diseases using an eye tracker. Different types of cataracts were implemented
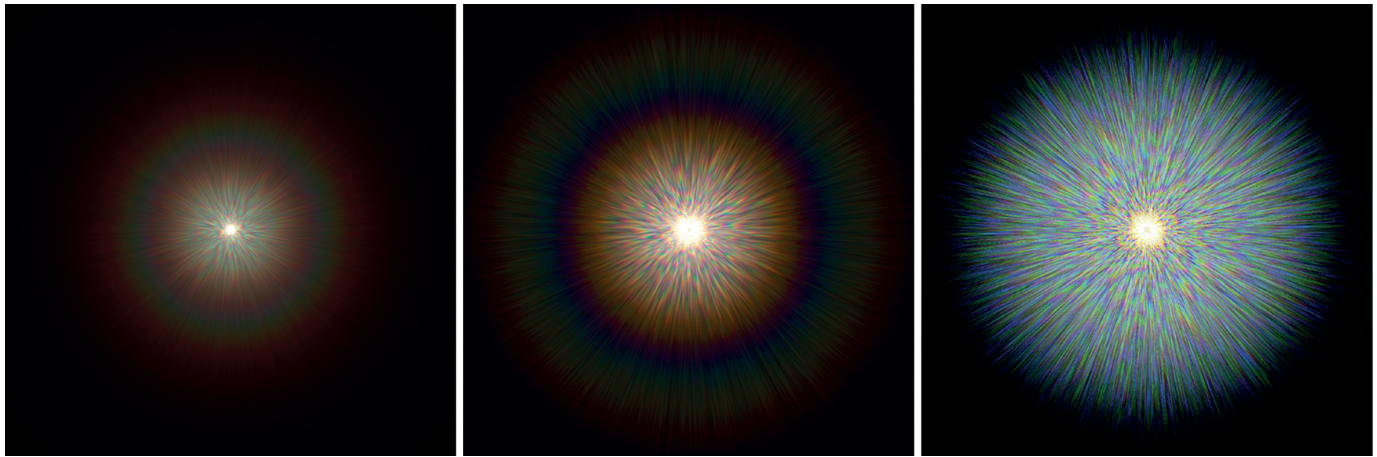
Fig. 2. Comparison of different glare kernels: Ritschel et al. [31] (left), ours (middle), and Berg et al. [39] (right).

to allow for better planning of escape route signs or placement of luminaries in a 3D scene. However, this approach does not include physically realistic simulation of glare or scotopic vision.

3.2   Simulating Bright Light Sources

Most common displays are not able to replicate the full range of brightness visible to humans. Therefore, to improve realistic perception, it is necessary to artificially increase the perceived brightness of the potentially dazzling parts of the image. The most straightforward solution to simulate bright light sources is a Gaussian convolution, i.e., a blur, applied to the bright pixels of a scene [46]. However, this blur does not approximate a real-world glare effect, but merely aims to generate a visually reasonable impression.

Algorithms generating a physically based glare effect [17, 31, 39] often make use of a PSF, which models the distribution of light on the retina in the eye. Kakimoto et al. [17] generated physically based glare images using Fraunhofer diffraction [13]. They used aperture masks and applied Fourier transforms to those masks at red, green and blue wavelengths. However, their approach is static and does not include real-time adaptations to changing parameters. Ritschel et al. [31] used the Fresnel approximation to Huygen's principle, which is a more generalized diffraction equation that includes Fraunhofer diffraction as a special case [13]. A single monochromatic PSF is created by the Fourier transform at a single wavelength and converted into a spectral PSF by averaging over multiple scaled copies along the visible human range. Their approach takes multiple influences into account, such as the pupil size, lens particles and gratings, vitreous particles and eyelashes. The perceptual glare effect implemented in our work builds upon this approach and adapts their method to run in real-time VR. Ritschel et al. [31] concluded that the glare perception could greatly vary between different users and there is no universally correct solution – we can support this statement with our user study results.

Effects proposed in other works are either based on static calculations or preset functions of the pupil size in regard to changes in lighting. In this work, we use an eye tracker to measure the user's changes in pupil size in real time and recalculate the glare kernel every frame based on that data. A comparison of three different glare kernels is shown in Fig. 2. We also use the eye-tracking data to modify the intensity of the effect depending on the gaze direction of the user, which gives a more realistic simulation than the other approaches.

Scandolo et al. [33] proposed a new real-time method for a more efficient calculation of the Fourier transform used to generate the PSF. This method works well on uniform circles or boxes. However, the authors do not include eye particles or other noise in their method.

None of these works included experiments comparing the simulated glare to a real-world situation during a user study. To the best of our knowledge, we are the first to let users rate a VR glare simulation and compare it to a glare effect perceived in the real world.

3.3   Luminance Adaptation

The brightness levels perceivable by humans range from $10^{-6} \frac{cd}{m^2}$ (faint starlight) to $10^8 \frac{cd}{m^2}$ (sunlight) [21]. However, the human eye needs to adapt to take in such a broad range. Larson et al. [22] proposed a global tone reproduction operator, based on local adaptation, using a histogram with real-world luminances, where 1 pixel represents $1°$ in the visual field. Ledda et al. [23] proposed a model for local eye adaption, which can be used as a static or temporal effect on high dynamic range (HDR) images and videos. Ferradans et al. [8] presented another model based on human visual adaptation. They extended the Naka-Rushton equation [34] to improve an image's local contrast similar to human vision.

3.4   Perceptual Tonemappers

When looking at recent research [7, 19, 46] regarding the perception of light and lighting situations, a very common topic is HDR tone mapping. The majority of the algorithms aim to compress HDR images as well as possible; however, they might neglect perceptual effects, like rod or cone vision. One of the most commonly used tonemappers was proposed by Reinhard et al. [30]. It uses a technique, inspired by traditional printing, that enhances contrast while compressing an image's luminance range. An early approach for perceptual tone mapping by Krawczyk et al. [18] took effects such as visual acuity, glare, and day and night vision into account. In contrast to other common tone-mapping algorithms, this method focuses not only on mapping the full contrast of an image onto a smaller range, but also includes visual effects that influence the perception of scenes. They used a Gaussian pyramid for all their implemented effects (temporal luminance adaptation, visual acuity and veiling luminance) due to the spatial similarities. We use a distinct glare method via a PSF which cannot be integrated into their workflow. To compute the loss of visual acuity, we apply a Gaussian blur to the lightness values in Lab color space, which is perceptually uniform, as opposed to Krawczyk et al., who blur the intensity values in CIE XYZ space. Additionally, we are still able to apply the loss of visual acuity in real time by splitting the kernel into two 1D filters.

Čadík [4] proposed a global and local hybrid method to achieve perceptually realistic tone-mapping results. Mantiuk and Markowski [24] employed an eye tracker to be able to simulate the human perception compression of light more accurately. Vangorp et al. [41] generated a local adaptation map based on their psychophysical experiments.

No other mentioned approach supports any adaptation to the gaze direction, since the works are mainly targeted at 2D images and videos. However, taking the view direction into account is crucial since it determines how much light enters the eye. Therefore, accurate simulations need to react to eye-tracking data.

Fig. 3. Initial scene adaption (left) compared to the fully converged scene adaption after 2.4 seconds (right).

4 SIMULATING HUMAN VISION

To simulate human vision as accurately as possible, perceptual algorithms need to respond to different lighting conditions in a similar way as the actual human eye. We identified the main influences on visual perception and consulted an optometrist for additional information on the processing of light in the eye. We conclude that the most significant influences on vision are the following:

- The **temporal eye adaptation** to bright and dark scenarios, due to the adaptation times of rods and cones.

- The **perceptual glare** we perceive when looking at bright light sources – colorful patterns that appear through the scattering of light in the eye, i.e., ocular straylight.

- In dark surroundings, specifically at less than $0.03 \frac{cd}{m^2}$, we experience a **visual acuity reduction** – edges blur, and details become harder to discern.

- **Scotopic color vision** (i.e., night vision) is significantly different from standard daylight vision – colors change in intensity and appear desaturated.

We apply these visual effects in different post-processing stages of a renderer in the above order.

4.1 Temporal Eye Adaptation

We calculate global temporal eye adaptation based on the scene luminances. This is done as the first post-processing step, so we can avoid the influence of other effects, such as glare, on our calculations.

We weight the linear RGB colors with a 2D Gaussian function centered at the gaze point obtained by the eye tracker. As a consequence, light sources in the periphery have little to no influence on our temporal adaptation. Then we downsample the scene to a size of 128×128 and generate a Gaussian pyramid down to 16×16 pixels. We then take the average over these 16×16 pixels and calculate the luminance Y (in $\frac{cd}{m^2}$) of the RGB value, using a D65 white point, after Poynton [28]:

$$Y = 0.2125 \cdot R + 0.7154 \cdot G + 0.0721 \cdot B. \qquad (1)$$

Following the equation of adaptation after Krawczyk et al. [18], the temporally filtered luminance L_i of the current frame i can be calculated as:

$$L_i = L_{i-1} + (Y - L_{i-1}) \cdot \left(1 - e^{-\frac{ft}{\tau(Y)}}\right) \qquad (2)$$

$$\tau(Y) = \sigma(Y) \cdot \tau_{rod} + (1 - \sigma(Y)) \cdot \tau_{cone} \qquad (3)$$

$$\sigma(Y) = \frac{0.04}{0.04 + Y}, \qquad (4)$$

where ft is the time that passed between the previous frame and the current one in seconds, and $\tau_{rod} = 0.4$ and $\tau_{cone} = 0.1$ are the adaptation times (in seconds) for rods and cones, respectively. The function $\sigma(Y)$ denotes the sensitivity of rods with regard to the luminance. This adaptation luminance L_i can then be applied to the image by multiplying it with the linear RGB values. This results in a gaze-dependent temporal adaptation to luminance over time (see Fig. 3).

4.2 Perceptual Glare

Light rays entering the eye scatter at different obstacles inside the cornea and lens, i.e., micrometer-sized particles (see Section 2). Some rays are redirected and hit the retina at a different spot than if going straight. This scattering creates a halo in our perception in the vicinity of bright light sources and can be modeled using a PSF.

4.2.1 The Point Spread Function

Our glare effect is based on the glare proposed by Ritschel et al. [31]. The performance of their approach was not sufficient to run in real time in VR or AR at the necessary minimum of 90 frames per second (FPS). We adapt this approach for a VR application, and make it view-dependent by using eye tracking. To achieve 90 FPS runtimes, we cut down expensive computations and only keep the minimum requirements for an accurate result. We consulted medical studies [9, 15, 32, 36, 39] and an optometrist and identified the parts of the algorithm that have the most influence on the final effect according to his medical expertise. We then adapted the approach accordingly, as shown in Table 1. The influence of the lens fibers is negligible, as these only have a low influence on light scattering. Furthermore, we

Table 1. Influences on glare perception and whether they were included in our algorithm. The anterior chamber was not included as influence for our glare simulation, because it induces no scattering for healthy eyes. The lens fibers and vitreous body were not included due to their low influence on the scattering of light in the eye.

Effect	Included
Cornea Particles	Yes
Anterior Chamber	No (no scattering)
Varying Pupil Size	Yes
Pupil Aperture	Yes
Lens Particles	Yes
Lens Fibers	No (low scattering)
Vitreous Body	No (low scattering)

Fig. 4. Simulation of a common glare phenomenon, with a pupil diameter of 4 mm, 1000 particles, particle diameter of 6 μm (left) and pupil diameter of 6 mm, 1000 particles, particle diameter of 10 μm (right). (Note that the faint rainbow-colored halo might be difficult to see on darker displays or prints.)
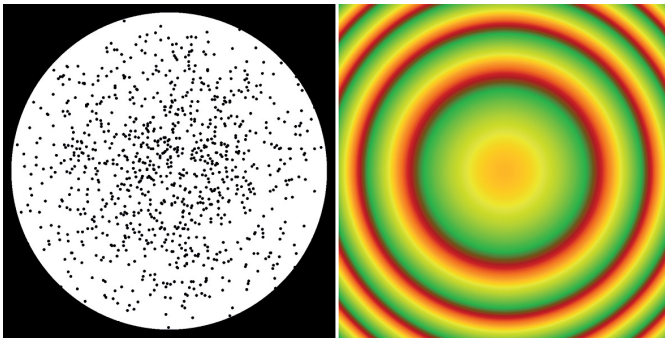
Fig. 5. Components of the PSF: simulated particles and aperture (left); complex Fresnel term remapped from [-1;1] to [0;1] for displaying (right).

chose not to include moving particles as these are mainly located in the vitreous humor, which hardly affects the human perception of glare.

We simulate particles inside the lens and cornea by generating a user-defined amount at random positions and projecting them onto a plane. In addition, the pupil size (aperture of the eye lens) is applied as a mask on the plane according to the actual user's pupil diameter. The resulting image is then converted to the spectral domain, following the principles of wave optics. Using this method, a spectral PSF is obtained, which can then be used as a glare kernel (see Fig. 4).

Particles   We focus our proposed model on the particles in the cornea and the lens of the eye, as those are two of the main influences on glare perception. In total, they account for around 70% of the glare phenomenon in the eye [31]. When a ray of light hits a particle in the eye, it scatters and gets bent along a specific angle. According to Ritschel et al. [31], the backward scattering of light, i.e., a bend angle greater than 90°, is "relatively unimportant" concerning glare. Therefore, we also neglect this property. When the forward scattered ray hits the retina, it has less intensity (due to the scattering) and is not aligned with the original path anymore. We perceive this as a faint glow around the light source. We simulate randomly distributed, static, circular particles on a 2D plane, which is a projection of the 3D eye space onto the pupil plane (see Fig. 5), as suggested by Ritschel et al. [31].

Pupil   The pupil of the eye resembles a camera aperture – it is a small opening in front of a sensor that only lets in a certain amount of light [27]. Different sizes of aperture allow for different lighting conditions, i.e., bigger pupils in a dark environment let more light into the eye. However, the more light enters the eye, the more stray-light occurs, and we perceive glare as more intense at night time [38]. Therefore, glare perception is highly dependent on the size of the pupil. The adaptation of the size of a human pupil to light and dark is done

automatically, involuntarily, and is continuously changing. In order to simulate glare realistically, this adaptation has to be taken into account. In contrast to Ritschel et al. [31], who calculate an artificial pupil size via time and field luminance, we use an eye tracker. We can measure the user's current pupil size and track the actual pupillary response of the user. Therefore, we are able to simulate the glare pattern in a more natural way. Similar to the particles, the pupil aperture is simulated in 2D space, as a simple circular opening. We calibrate our eye tracker to a user's pupil size by showing a black or white screen for 5 seconds each. We take the average of the pupil size during the white frame as minimum pupil size and the average over the black frame as maximum. At runtime, we then generate the pupil aperture by mapping the eye tracker output to our predefined range of 2–8 mm diameter. Finally, we multiply it with the simulated particles, as shown in Fig. 5, left.

Wave Optics   In order to transform the simulated particles and the aperture (i.e., the aperture mask) into an actual spectral PSF, we use an approach based on wave optics, as proposed by Kakimoto et al. [17]. Wave optics aim to describe the interference and the scattering of light in a physical way. The authors base their approach on the diffraction of light on obstacles, such as the pupil aperture, to simulate the incident light in the human eye. They show that the Fraunhofer diffraction equation can be transformed into an equation with a Fourier transform for the integral, which can be solved in real time with a 2D Fast Fourier transformation (FFT):

$$I_f\left(x_f, y_f\right) = \frac{A^2}{\lambda^2 f^2} \left|\mathscr{F}\left[t_0\left(x_0, y_0\right) P\left(x_0, y_0\right), \lambda f\right]\right|^2, \quad (5)$$

where I_f is the resulting PSF at coordinates (x_f, y_f), A is the amplitude of the wave, λ is the wavelength, f is the focal distance and $t_0(x_0, y_0)$ is an image masked by the pupil function $P(x_0, y_0)$. This approach can be enhanced by adding a Fresnel term (see Fig. 5, right), according to Ritschel et al. [31], which is more accurate than Fraunhofer diffraction, due to the short distance between the pupil and the retina.

4.2.2   Glare Kernel Generation

For generating the glare kernel, we evaluate all of the following equations in the normalized device coordinate space, where $x, y = [-1; 1]$. The subscript $\mathbb{C}$ denotes complex numbers. The generation of the glare kernel consists of the following steps.

Generation of static particles   In a pre-processing step, the two-dimensional static particles $P(x, y)$ are generated as a binary random dot pattern with constant particle/dot size s.

Calculation of static Fresnel term   The static Fresnel term, following Huygen's principle after Ritschel et al. [31], is defined as

$$F_{\mathbb{C}}(x, y) = e^{\,\mathrm{i}\frac{\pi}{\lambda d}\left(x^2 + y^2\right)}, \quad (6)$$

where λ is the wavelength and d the distance from the pupil to the retina. In order to avoid having to calculate an FFT for every visible wavelength, the mean value of the human perceivable spectrum is used, specifically $\lambda = 575$ nm. Furthermore, $d = 24$ mm is used as the human focal length [14].

Generation of varying pupil aperture   At runtime, the pupil aperture $A(x, y)$ is generated, depending on the currently measured pupil size of the user as binary mask.

Lens equation   The three functions above are then multiplied, which results in the complete lens equation for simulating glare effects:

$$L_{\mathbb{C}}(x, y) = P(x, y) \cdot F_{\mathbb{C}}(x, y) \cdot A(x, y). \quad (7)$$

Fourier transformation to monochromatic PSF   We then transform this equation into frequency space to generate the monochromatic PSF. We can define the monochromatic PSF $M(x, y)$ after Ritschel et al. [31] as:

$$M(x, y) = \frac{1}{(\lambda d)^2} \left|\frac{1}{N} \cdot \mathscr{F}\left[L_{\mathbb{C}}(x, y)\right]\right|^2, \quad (8)$$

where N is the size of the input. The complex output of the Fourier transform is normalized by the image size, wavelength λ and pupil length d. The result is a single-channel 2D image, representing the scattered, incoming light on the retina for a single wavelength.

Conversion to spectral PSF   The spectral PSF is generated by summing up $M(x,y)$ at different wavelengths φ_i in nanometers of the visible human range:

$$S_{\text{XYZ}}(x,y) = \frac{1}{k+1} \cdot \sum_{i=0}^{k} \text{nm2XYZ}(\varphi_i) \cdot M\left(x\frac{\lambda}{\varphi_i}, y\frac{\lambda}{\varphi_i}\right), \quad (9)$$

$$\varphi_i = 380 + \frac{i}{k}(770 - 380), \quad (10)$$

where k is a constant that defines the "fineness" of the interpolation and nm2XYZ is the conversion from a wavelength in nanometers to the XYZ color space. We multiply the intensity of the incoming light at $M\left(x\frac{\lambda}{\varphi_i}, y\frac{\lambda}{\varphi_i}\right)$ with the XYZ color of the respective wavelength after Wyman et al. [44]. By using XYZ colors, we get a perceptually based average for each pixel. Finally, the image, S_{XYZ}, is transformed into linear RGB space and results in the spectral RGB kernel $S_{\text{RGB}}(x,y)$, which can then be used as glare kernel.

4.2.3 Convolutional Bloom

The glare kernel, as described in Sect. 4.2.2, is applied to the image using a convolutional FFT bloom, where both image and kernel are transformed to the frequency domain and multiplied. The result is then transformed back into linear RGB image space. This approach does not only blend the rendered image smoothly with our glare kernel, but also results in different glare intensities, depending on the intensity of the light source. Since we need two FFTs per eye (forward and inverse) and another one for the kernel, this results in five 2D FFT transformations per frame (in addition to the first transformation of the lens function into the kernel), which is very costly and not well suited for real-time VR or AR applications. According to the optometrist we consulted, the glare intensity heavily depends on the current gaze direction. Therefore, we apply our bloom effect according to the user's gaze direction in a smaller window (to save computation time) and blend it with a Gaussian falloff over the original image. In contrast to Ritschel et al. [31], who apply the glare effect uniformly over the whole image, we achieve less pronounced glare effects in the periphery and more intense effects in close proximity to the gaze point of the user. Therefore, we are able to approximate human perception more accurately, because the perceived glare is greatly influenced by our viewing direction [11]. The glare phenomenon is more intense when looking directly at a light source.

Since our eyes never stay still, we also do not see a glaring light as a purely static phenomenon. The perceived movement of a glare mainly comes from constant unconscious movements of the eye, so-called microsaccades. We include all microsaccades our eye tracker detects in our simulation just like normal eye movement. (See Sect. 7.2 for further details.)

4.3 Visual Acuity Reduction

Human visual acuity is highly dependent on the illumination in a scene. With decreasing luminance values, the perceived acuity is reduced as well. To simulate this phenomenon, a simple blur can be applied to a rendered image, depending on the current point of focus. However, we use a more sophisticated method for the whole simulated image – we blur the brightness values depending on a visual acuity function. Since this automatically leads to different intensities of reduced visual acuity in darker and brighter areas of the image, no additional knowledge of the viewing direction is necessary.

4.3.1 Loss of Visual Acuity

In our approach, we simulate the loss of visual acuity based on the method proposed by Krawczyk et al. [18]. In a post-processing step, we convert the linear HDR values (i.e., before tone mapping) of the image

to the Lab color space, where L is the lightness of the pixel. Then the lightness values are blurred, in horizontal and vertical direction. The intensity of the blur for each pixel aims to approximate the function fit of real foveal acuity data, as proposed by Larson et al. [22]. This approach results in a small error, due to the non-uniform blur kernel, yet this can be neglected, as shown in Sect. 4.3.3. Converting the processed values back to RGB colors results in an image where dark regions are blurred.

The reduction of visual acuity consists of the following steps:

1. Convert linear HDR RGB values to Lab color space

2. Horizontal pass: blur L (lightness) with 1D Gaussian blur kernel, with sigma dependent on the lightness value

3. Vertical pass: blur L again with 1D Gaussian blur kernel, with sigma dependent on the (new) lightness value

4. Convert Lab colors back to linear RGB color space

While in some special cases this can result in Lab values that cannot be represented in the sRGB space and need to be clamped, we conclude – due to our perceptual evaluation – that this does not yield any obtrusive irregularities.

4.3.2 New Function Fit

We propose a faster function fit to approximate the loss of visual acuity in the dark. This is relevant due to the high performance necessary for VR applications. The original formula by Krawczyk et al. [18] is given by:

$$\sigma(L) = \frac{width}{fov \cdot 1.86 \cdot \sqrt{2} \cdot R(\text{LtoY}(L))}, \quad (11)$$

where $\text{LtoY}(L)$ is the conversion from L in Lab to Y in XYZ color space, $width$ the width of the rendered image, fov the horizontal field of view (FOV) in degrees and R the function fit proposed by Larson et al. [22] to calculate the maximum perceivable visual acuity. The resulting σ^2 denotes the variance for the 2D Gaussian blur. We approximate this by:

$$\sigma(L) = \max(1 - L, 0). \quad (12)$$

A comparison of the two functions is shown in Fig. 6. In bright regions of the image, the visual acuity stays unchanged, therefore, $\sigma = 0$ is reasonable. However, in the dark regions of the image, visual acuity reduction takes place up to a variance of $\sigma = 1$. The benefit of this function is that no blur is applied at lightness values greater than one because our function is zero for those values. In very bright areas, there is no significant difference in human visual acuity anyhow. Furthermore,
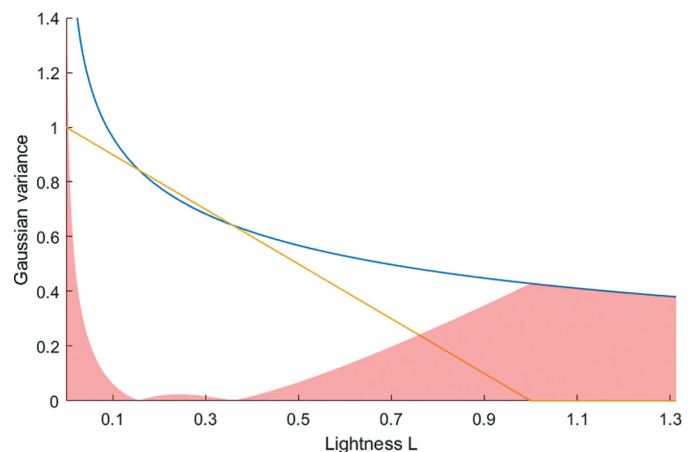
Fig. 6. Comparison of Gaussian variance σ, for different lightness values, of Krawczyk et al. [18] (blue) and our approach (yellow). The absolute difference is marked as red region.
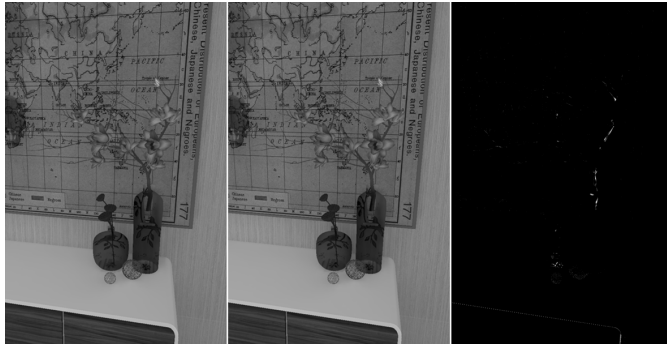
Fig. 7. Comparison of the lightness of an image when applying a 2D visual acuity filter (left) vs. two 1D filters (middle). The absolute difference between the two is shown on the right.

the maximum displayable acuity per eye of our VR headset, the *HTC Vive Pro*, is $\frac{width}{fov} = \frac{1440}{104} \approx 13.85$ pixel per degree (PPD). By rewriting the original function fit from Larson et al. [22] we get

$$L = \text{YtoL}\left(\exp\left(-1.64 \cdot \tan(1.49 - 0.06 \cdot R) - 0.575646\right)\right). \quad (13)$$

Setting $R = 13.85$, we can conclude that the highest displayable resolution of our HWD corresponds to the visual acuity of a human at $L \approx 1.31$. The perceived visual acuity of real-world lightness values $L > 1.31$ cannot be displayed in our HWD due to the limitations of the hardware. Therefore, our new approximation is able to replicate real-world acuity reasonably, even though we only handle $L \leq 1$. Differences in visual acuity in brighter regions would be too small to display in our HWD anyhow. Our function leads to fewer computations necessary at bright pixels or generally for a bright image. The maximum of our approximation, $\max(\sigma(L))$, is 1 at $L = 0$. This upper bound occurs because the Lab system allows no negative lightness values. This is well suited for real-time applications because an upper function boundary leads to an upper limit for a convolution kernel size. Following the common rule of $s = 2 \cdot \lfloor 3 \cdot \sigma \rfloor + 1$ for the kernel size s [26] gives a maximum size of 7, which proved to be sufficient in our user study for a realistic simulation of loss of visual acuity in VR.

4.3.3 Applying the Blur

Since the application of a 2D blur kernel is not well suited for real-time applications, we separate the 2D kernel into two 1D kernels. Due to the varying size of the blur kernel for every pixel, errors are induced at the edges between bright/dark changes of the filtered image. Furthermore, additional irregularities occur by determining the filter size of the second pass based on the already 1D-filtered image. Both of these errors are minimal and hardly recognizable with the human eye, as shown in Fig. 7. Using the previously applied FFT to remove frequencies and therefore achieve a blur is not possible in this case, as we blur each pixel with an individual sigma, depending on its brightness.

4.4 Scotopic Color Vision

Scotopic color vision describes the color shift we perceive in darker environments. We implement scotopic color vision by adding a color shift that depends on the temporally adapted scene luminance calculated beforehand (see Section 4.1). The absolute scotopic sensitivity of photorecptors for a given luminance in the scene is taken into account – the more sensitive the rods (and thus the less sensitive the cones), the more intense the color shift. We calculate this after tone mapping. If the intensity of incoming light is too low to trigger the (mainly red and green-sensitive) cones, rod-vision is activated. Then, mostly rods and blue-sensitive cones are enabled, leading to a color shift, because colors like blue and purple are the most intense in this case. In our simulation, we apply a color shift towards a lavender purple color, after Krawczyk et al. [18], because of the perceptual change towards light blue to purple at night. We use the original scene luminance (i.e., not tone-mapped)

and the sensitivity of rods, given by Equation 4. Depending on this sensitivity, we add a color shift such that

$$SV = RGB \cdot (1 - \sigma(L_i)) + [1.05, 0.97, 1.27] \cdot L_i' \cdot \sigma(L_i), \quad (14)$$

where RGB is the tone-mapped LDR color, L_i the temporally filtered luminance of the current frame, L_i' the tone-mapped luminance and $[1.05, 0.97, 1.27]$ the purple tint.

5 USER STUDY

To evaluate the realism of our simulation, we conducted a user study with five participants, aged 23 to 32, where one participant was female and four were male. One of the participants wore glasses (also in the HWD), two wore contact lenses, and another two had no visual aid at all. One participant had very slight deuteranomaly (red-green color vision deficiency), but described it as barely noticeable in their everyday life. In this pilot study we focused on collecting qualitative feedback of a few participants to investigate differences of human vision in real life and VR. We did not aim to obtain extensive statistical data, but detailed verbal feedback from the participants to improve our simulation in future work. During our experiments users were asked to compare a real-world low-light scene to a similar virtual scene, modified with our simulation, in VR and rate its realism. The user study protocol consisted of the following parts:

Study Information   We explained the aim and general procedure of our study to the participant.

Real-World Experiment   To create a reference for comparison to our VR scene, we set up a real-world low-light scene, see Fig. 8. We asked the participants a few questions about their perception, for example: What does the glare look like? How does it change when you move around the room? How do you perceive the colors of the scene?

Eye Tracker Calibration   The participant put on the HWD and we started the eye tracker calibration. First, they had to look at a green dot circling the center of the display to calibrate the viewing direction. Second, we showed a black screen and a white screen for 5 seconds each to calibrate the pupil size (as described in Sect. 4.2.1).

VR Experiment   We showed the participant a low-light glare scene in VR and asked them to compare our simulation to their memory of the real-world experiment before. They could freely explore the VR scene and analyze the differences. We used an office scene with only a single desk lamp as light source.

Questionnaire   We asked the user to compare the simulation to their real perception while they were still in VR. They rated all implemented effects on a Likert Scale and gave verbal feedback on perceived differences and explained their ratings.

Fig. 8. Real-world setup. Note that the human perception of a real-world scene is different than a photograph.
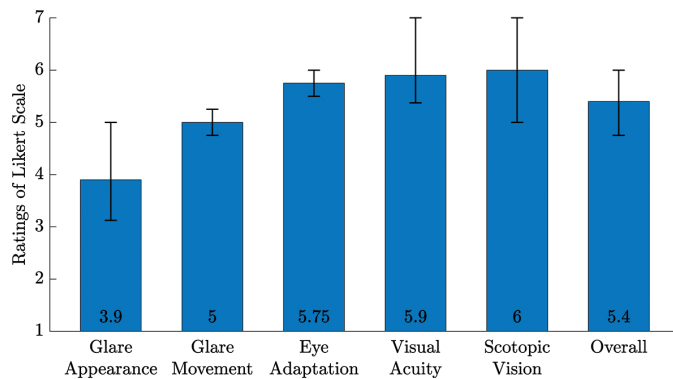
Fig. 9. Average user study ratings of five participants, where one means "completely different" and seven stands for "exactly the same". The small bars represent the 25% and 75% percentile respectively.

6 RESULTS

All participants were asked to rate six different categories on a Likert Scale from one to seven, where one means "completely different" and seven stands for "exactly the same", when comparing their real perception during the real-world experiment to their perception in the VR simulation. They were asked to evaluate and to explain their decisions considering the following categories:

Glare Appearance How does the effect of the glare around a bright light source look like?

Glare Movement When moving around the scene, or not looking straight at the glare, how does the glare change?

Eye Adaptation How does the illumination change when looking from bright to dark regions or vice versa?

Visual Acuity How well are the details in dark regions perceived?

Scotopic Vision How do the colors change in dark regions?

Overall How would you rate the overall scene?

Fig. 9 shows the average rating of all participants per category.

6.1 Qualitative Feedback

During the experiments, users were also asked to give reasons for their rating in each category.

Glare Appearance   Regarding the glare appearance, in general, all participants stated that their perception of glare in the real world was much more delicate regarding light streaks and much more detailed than our simulated glare. It was noted multiple times that the corona or the center of the glare seemed too intense in VR. Furthermore, the colors were described as too intense and saturated in VR. They appeared more reddish in VR than in real life, and the center of the glare appeared whiter when looking at the real-world scene. However, some participants stated that the rainbow-like circles on the outside of the glare were very realistic and similar to their perception. One participant noted that they perceived more colored circles in real life than in VR – this, therefore, seems to be a very user-specific phenomenon. Additionally, it was mentioned by one participant that their vision of glare was much more circular and less jagged than our simulation. Furthermore, one person noted that they found the slight pulsing of the glare irritating and disturbing. They described their glare perception as more fluid, like water, while they perceived the VR simulation as too jerky. In contrast, another participant mentioned that the pulsation of the glare in VR seemed very nice, while not entirely similar to their real perception; they still deemed it a realistic effect.

Glare Movement   The participants were asked to rate the appearance of the animation of the glare when moving around in the scene or changing gaze direction. One participant claimed the glare disappeared too quickly when glancing away from it, another one claimed it was still too intense when focusing on something nearby. Another person rated the effect of eye movement in the scene to be just perfect. One participant stated that they perceived fewer colors when looking away from the light in real life, while the simulation did not change color at all. Additionally, it was mentioned multiple times that the glare effect did not seem to tilt correctly with the user, i.e., the participants expected some deformation when viewing the glare from the sides, but our simulated glare stayed circular.

Eye Adaptation   The effect of eye adaptation was commented on very positively, i.e., most participants said it resembled their perception a lot, it seemed natural and they were very comfortable with it. The main point of critique was that the adaptation from bright to dark scenes was too slow.

Visual Acuity   The effect "loss of visual acuity in dark areas" was rated as entirely equal to their perception in real life by four out of five participants. All of those noted that they hardly had noticed it at all before being asked to rate it. One participant added that when viewing a dark scene, more "noise", i.e., irregularities, should appear.

Scotopic Vision   For the evaluation of the implemented color shift in scotopic vision, two participants noted that the colors completely matched their perception in a dimly lit scene. Another one noted that the scene, in general, seemed to be very warm with brown and red colors – therefore, the color shift in the dark areas seemed too intense. On the other hand, another participant mentioned that they thought the colors of the darker regions were too intense, i.e., they said a more intense shift would be necessary.

Overall   Overall, most participants rated our simulation above average. One participant rated it to be neither good nor bad, all the others found it good or very good. However, no one rated it as perfect. Three out of five participants noted that all the effects were harmonious and generated a realistic scene. Some participants mentioned that, in VR, the lamp as a light source was not visible behind the intense glare, while in reality, the lamp was visible.

6.2 Comparison to Default Rendering Settings

When comparing an image of a low-light scene generated by a default renderer to our implementation, as shown in Fig. 1, the differences can clearly be seen. (Note that our simulation will be perceived differently inside an HWD, especially because of the different field of view.) While the perception of the quality of the improvements is subjective, we argue that our approach is able to replicate low-light and glare better than standard rendering. To verify this statement, we questioned the participants – subsequent to our original user study – about their perception when comparing our adaptation to a "default" rendering process, e.g., as provided by Unreal Engine 4 (UE4). Participants were given two videos (one with our simulation, one with UE4 default rendering) to compare. They rated our simulation as 4.6 (on average) on a 7-point Likert Scale, and 3 (on average) for the default rendering, in terms of realism. Four out of five participants preferred our simulation.

6.3 Runtimes

We also evaluated the performance of our simulation for VR/AR applications. Our simulation can run in real time on current PCs and has robust performance on high-end hardware. The rendering times, on a PC with an *NVIDIA GTX 1070* graphics card, for different stages of our method are shown in Table 2.

Table 2. Runtimes for different rendering stages. The overall GPU frame time includes all operations necessary to render one frame.

Stages	Count	Avg. GPU times
Aperture	Once per frame	0.04 ms
Spectral PSF	Once per frame	2.34 ms
Visual Acuity Reduction	Per eye	0.36 ms
Temporal Eye Adaptation	Per eye	0.18 ms
Glare Convolution	Per eye	1.47 ms
Scotopic Colors	Per eye	0.14 ms
Overall Post-Processing	Per eye	2.42 ms
Overall GPU	All-together	9.57 ms

Fig. 10. Low-light 360° HDR image (top) and with our proposed adaptations (bottom).

7 DISCUSSION AND LIMITATIONS

In this section the results and hardware constrains are discussed.

7.1 Discussion of Results

Most user-study participants agreed on the main arguments, like the glare appearing as too coarse and intense, or the proper simulation of night vision. Some outliers confirmed our assumption that human perception is highly subjective. Therefore, it is difficult to generate a generally acceptable model. We argue that a method that allows individual adjustment of each effect for each user, like the one we propose, could overcome this problem.

Furthermore, the results of our user study showed that the most significant improvements for future work could be made regarding the glare. Other phenomena, like scotopic vision and temporal adaptation, have already been widely researched [4,8,18] and by building upon this research, we were able to generate plausible simulations. Glare effects are highly dependent on the internal eye anatomy, like particle count and size, which greatly varies from person to person and cannot be measured without specialized equipment. Therefore, simulations need to be adapted to the perception of the individual user to increase the visual quality of the simulation for them. We can adapt our simulation to external eye parameters like pupil size and view direction, but did not yet evaluate modifying parameters such as particle size and count at run-time with users. In future work, even more adjustable parameters could be integrated into our simulation. However, this would require substantial medical measurements of the characteristics of the user's eye, and calibrations beforehand.

The eye tracker generated volatile data for two participants due to glasses or mascara worn during the user study. This resulted in heavy flickering of the simulated glare – zero was returned as pupil size when the pupil could not be detected in that frame, which lead to unrealistic results. Our algorithm was not able to adapt to this unstable data and should be improved in this direction.

All user-study participants mentioned that the simulated glare seemed too "thick" and unnatural. While this might be an issue in the algorithm, it has to be mentioned that the used VR-HWD is not able to display details at the same high resolution as the human eye can perceive them. The *HTC Vive Pro* has a PPD value of 13.85, while the human eye at 20/20 vision can perceive approximately 60 PPD [35].

Another limitation of our work is that the glare kernel is always based on an equal-energy light, independent of the rendered light's color. Different colors and, therefore, wavelengths of light influence the perceived glare in different ways. While in theory, convolving the glare kernel with colored light should influence the final output color, this happens only very slightly and does not sufficiently resemble the perceived glare of colored light in the real world.

One element not yet included in our simulation was the influence of eyelashes on the perception. Our eye tracker is able to detect blinking, with a duration of on average 300–400 ms [42]. Due to a decreasing or increasing pupil size detected during the eyelid movement, our glare kernel adapts in some way to a blink of the eye. However, the influence of eyelashes interfering with the incident light was not accounted for in our current implementation. Surprisingly, none of the user study participants mentioned this phenomenon as "missing" or described any differences noticed.

7.2 Hardware constraints

Vive Pro cameras The proposed workflow can also be used to modify a video stream for video-see-through AR applications. Due to the low quality of the front cameras of the *HTC Vive Pro* (640×480 px, no HDR), we cannot display a video-see-through AR stream (modified with our simulation) in an HWD that is comparable to a real-world scene. However, applying our method to 360° images or videos, as shown in Fig. 10, allows us to demonstrate the AR capabilities of our method.

Display The AMOLED display of the *HTC Vive Pro* is able to display luminances from 0.04 to $130 \frac{cd}{m^2}$ [5], while the human visual system ranges from approximately 10^{-6} to $10^8 \frac{cd}{m^2}$. Two out of four of our effects – loss of visual acuity and scotopic color vision – only appear in scotopic vision, which sets in at luminances smaller than $0.03 \frac{cd}{m^2}$, hence is outside the displayable range of the HWD. Additionally, in our real-world experiment, we used an LED as glare source, with a luminance of approximately $5 \times 10^7 \frac{cd}{m^2}$, which is also outside of the displayable range of our HWD. Further, temporal adaptation occurs constantly in the human eye, but since the luminance range of the HWD is much smaller than the humanly perceivable range, this effect also needs to be simulated accordingly. Ideal VR headsets should be able to replicate the whole human visual system. However, having a pixel as bright as the sun a few centimeters away from the human eye is not reasonable. Hence, we need techniques to simulate bright and potentially harmful luminances safely, as well as very low light intensities.

Eye tracker We used the *Pupil Labs HTC Vive Binocular Add-on* eye tracker with a tracking frequency of 200 Hz, a gaze accuracy of $\sim 1.0°$, precision of $\sim 0.08°$ and camera latency of 5.7 ms. Our eyes perform constant unconscious movement, called microsaccades, which are approximately 10 ms long. Therefore, the eye tracker is, in theory, able to detect these microsaccades. However, it uses a confidence value to filter out noise, potentially also filtering out some microsaccades. Ehinger et al. [6] investigated the capabilities of the Pupil Labs eye tracker (with 120 Hz cameras) and found that it is able to detect approximately 50 percent of microsaccades. Hence, it is reasonable to assume that our eye tracker, which features two 200 Hz cameras is able to detect more than 50 percent of all microsaccades. However, this needs to be evaluated in future work.

8 CONCLUSION

In this paper, we propose a tool for simulating the perception of light in VR. We modified the glare methodology proposed by Ritschel et al. [31] to run in real-time VR and AR. Additionally, we used eye tracking to enable our simulation to react to the user's viewing direction and pupil

size. We also incorporated an adaption of the work by Krawczyk et al. [18] into our framework, in order to add more realism in low-light scenes. Our work has made improvements to standard simulations of low-light scenes and added further realism to the simulation of glare. The results of our pilot study indicate that our developed application can simulate temporal eye adaptation, reduced visual acuity and scotopic color vision similar or very close to what humans perceive in real-life situations. To the best of our knowledge, our glare effect is the first perceptual glare effect that combines real-time performance, an online PSF, and a sound basis in medical research. We also identified areas of improvement for glare appearance and glare movement to increase realism even further in future work. With our user study, comparing a real-life situation to a VR simulation, we were able to show the importance of medically based, perceptual effects to increase the quality of visual perception in VR, which leads to more realism of the simulation and potentially also better immersion. Our work can be added to any standard real-time rendering tool or framework as independent post-processing steps for each effect or as a general post-processing tool.

9 FUTURE WORK

We have identified the following possibilities to further improve the realism of our simulation in future work.

Multiple user-study participants noted that the glare they perceived in real life was more delicate than in our simulation – we could try to generate more detailed light streaks by using bigger textures for the generation of the glare kernel. To add more perspective to the glare, we could render the glare kernel on a semi-transparent plane in front of the light source, also reducing the number of costly FFTs. However, this approach would only be well suited for point lights, not area lights. A prominent effect that has not been accounted for in this work are so-called afterimages or after effects [27]. With a more detailed simulation of the absorption and reproduction of the photoreceptors, the simulation of these effects could further increase the realism of a VR simulation. Additionally, erroneously firing rods during low lighting ambiance leads to perceived noise in the human visual system, which could easily be added as a filter and might increase realism further.

Our perceptual glare is already used in vision impairments simulations [20] to simulate sensitivity to light as experienced by cataract patients. Further refinements of the glare characteristics for different vision impairments could help improve these simulations and enable studies on lighting design tailored to people with vision impairments.

Larger user studies should be conducted on the topic of light simulation to allow for a direct comparison of the perceived phenomena to simulated phenomena. Further assessment of the glare appearance on rendered images could be done on an HDR display to be able to look at the rendered glare and a real-life situation at the same time and compare them. Applying our simulation to real-world HDR images and comparing it to a user's perception, similar to Wienold and Christoffersen [43] or Yoshida et al. [45], would allow further investigations on the accuracy of our implementation. The comparison of a real-world scene to an AR simulation could give further insights into the differences of real-world perception and the perception inside an HWD.

ACKNOWLEDGMENTS

REFERENCES

[1] G. B. Airy. On the diffraction of an object-glass with circular aperture. *Transactions of the Cambridge Philosophical Society*, 5:283, 1835.

[2] M. Bass, C. DeCusatis, J. Enoch, V. Lakshminarayanan, G. Li, C. Macdonald, V. Mahajan, and E. Van Stryland. *Handbook of optics, Volume II: Design, fabrication and testing, sources and detectors, radiometry and photometry*. McGraw-Hill, Inc., 2009.

[3] E. Britannica. Sensory reception: human vision: structure and function of the human eye. *Encyclopedia Brittanica*, 27:179, 1987.

[4] M. Čadík. Perception motivated hybrid approach to tone mapping. *International Conference in Central Europe on Computer Graphics, Visualization and Computer Vision*, 2007.

[5] O. Clausen, G. Fischer, A. Furhmann, and R. Marroquim. Towards predictive virtual prototyping: Color calibration of consumer vr hmds. In *16th GI AR/VR Workshop*, 2019.

[6] B. V. Ehinger, K. Groß, I. Ibs, and P. König. A new comprehensive eye-tracking test battery concurrently evaluating the pupil labs glasses and the eyelink 1000. *bioRxiv*, 2019. doi: 10.1101/536243

[7] G. Eilertsen, J. Unger, and R. K. Mantiuk. Chapter 7 - evaluation of tone mapping operators for hdr video. In F. Dufaux, P. L. Callet, R. K. Mantiuk, and M. Mrak, eds., *High Dynamic Range Video*, pp. 185–207. Academic Press, 2016. doi: 10.1016/B978-0-08-100412-8.00007-3

[8] S. Ferradans, E. Provenzi, M. Bertalmio, and V. Caselles. Tstm: A two-stage tone mapper combining visual adaptation and local contrast enhancement. *IMA Preprint Series # 2253*, 2009.

[9] L. Franssen and J. E. Coppens. *Straylight at the retina : scattered papers*. PhD thesis, University of Amsterdam, 2007.

[10] L. Franssen, J. Tabernero, J. E. Coppens, and T. J. T. P. van den Berg. Pupil size and retinal straylight in the normal eye. *Investigative Ophthalmology & Visual Science*, 48(5):2375–2382, 1 2007. doi: 10.1167/iovs.06-0759

[11] G. A. Fry and M. Alpern. The effect of a peripheral glare source upon the apparent brightness of an object. *Journal of the Optical Society of America*, 43(3):189–195, 1953. doi: 10.1364/JOSA.43.000189

[12] H. S. Ginis, G. M. Perez, J. M. Bueno, A. Pennos, and P. Artal. Wavelength dependence of the ocular straylightwavelength dependence of the ocular straylight. *Investigative Ophthalmology & Visual Science*, 54(5):3702–3708, 1 2013. doi: 10.1167/iovs.13-11697

[13] J. W. Goodman. *Introduction to Fourier optics*. Roberts and Company Publishers, 2005.

[14] E. Hecht. *Optics*. Pearson education. Addison-Wesley, 2002.

[15] K. Irsch and D. Guyton. Anatomy of eyes. *Encyclopedia of Biometrics*, 1 2009. doi: 10.1007/978-0-387-73003-5_253

[16] N. L. Jones and C. F. Reinhart. Real-time visual comfort feedback for architectural design. In *PLEA 2016 Los Angeles–32nd International Conference on Passive and Low Energy Architecture*, pp. 659–664, 2016.

[17] M. Kakimoto, K. Matsuoka, T. Nishita, T. Naemura, and H. Harashima. Glare generation based on wave optics. In *Proceedings - Pacific Conference on Computer Graphics and Applications*, pp. 133–142, 2004. doi: 10.1109/PCCGA.2004.1348343

[18] G. Krawczyk, K. Myszkowski, and H. P. Seidel. Perceptual effects in real-time tone mapping. In *Spring Conference on Computer Graphics, SCCG 2005 - Conference Proceedings*, pp. 195–202, 2005. doi: 10.1145/1090122.1090154

[19] K. Krösl, C. Elvezio, M. Wimmer, M. Hürbe, S. Feiner, and S. Karst. Icthroughvr: Illuminating cataracts through virtual reality. In *26th IEEE Conference on Virtual Reality and 3D User Interfaces, VR 2019 - Proceedings*, pp. 655–663. Institute of Electrical and Electronics Engineers Inc., 3 2019. doi: 10.1109/VR.2019.8798239

[20] K. Krösl, C. Elvezio, L. R. Luidolt, M. Hürbe, S. Karst, S. Feiner, and M. Wimmer. CatARact: Simulating cataracts in augmented reality. In *2020 IEEE International Symposium on Mixed and Augmented Reality (ISMAR)*. IEEE, 2020.

[21] T. Kunkel, S. Daly, S. Miller, and J. Froehlich. Chapter 15 - perceptual design for high dynamic range systems. In F. Dufaux, P. L. Callet, R. K. Mantiuk, and M. Mrak, eds., *High Dynamic Range Video*, pp. 391–430. Academic Press, 2016. doi: 10.1016/B978-0-08-100412-8.00015-2

[22] G. W. Larson, H. Rushmeier, and C. Piatko. A visibility matching tone reproduction operator for high dynamic range scenes. *IEEE Transactions on Visualization and Computer Graphics*, 3(4):291–306, 1997. doi: 10.1109/2945.646233

[23] P. Ledda, L. P. Santos, and A. Chalmers. A local model of eye adaptation for high dynamic range images. In *Proceedings of the 3rd International Conference on Computer Graphics, Virtual Reality, Visualisation and Interaction in Africa*, AFRIGRAPH '04, pp. 151–160. ACM, New York, NY, USA, 2004. doi: 10.1145/1029949.1029978

[24] R. Mantiuk and M. Markowski. Gaze-dependent tone mapping. In *Lecture*

Notes in Computer Science (including subseries Lecture Notes in Artificial Intelligence and Lecture Notes in Bioinformatics), vol. 7950 LNCS, pp. 426–433, 2013. doi: 10.1007/978-3-642-39094-4_48

[25] B. Meyer, S. Grogorick, M. Vollrath, and M. Magnor. Simulating visual contrast reduction during nighttime glare situations on conventional displays. *ACM Trans. Appl. Percept.*, 14(1):4:1–4:20, 7 2016. doi: 10.1145/2934684

[26] H. Nguyen. *Gpu Gems 3*. Addison-Wesley Professional, first ed., 2007.

[27] S. E. Palmer. *Vision science: Photons to phenomenology*. MIT press, 1999.

[28] C. Poynton. Frequently asked questions about gamma. *Rapport Technique, janvier*, 152, 1998.

[29] D. E. Purves, G. J. Augustine, D. E. Fitzpatrick, W. C. Hall, A.-S. E. LaMantia, J. O. McNamara, and L. E. White. Neuroscience. *Sinauer associates*, 2008.

[30] E. Reinhard, M. Stark, P. Shirley, and J. Ferwerda. Photographic tone reproduction for digital images. *ACM Trans. Graph.*, 21(3):267–276, 7 2002. doi: 10.1145/566654.566575

[31] T. Ritschel, M. Ihrke, J. R. Frisvad, J. Coppens, K. Myszkowski, and H.-P. Seidel. Temporal glare: Real-time dynamic simulation of the scattering in the human eye. In *Computer Graphics Forum*, vol. 28, pp. 183–192, 2009.

[32] J. J. Rozema, T. J. T. P. den Berg, and M.-J. Tassignon. Retinal straylight as a function of age and ocular biometry in healthy eyes. *Investigative Ophthalmology & Visual Science*, 51(5):2795–2799, 1 2010. doi: 10.1167/iovs.09-4056

[33] L. Scandolo, S. Lee, and E. Eisemann. Quad-based fourier transform for efficient diffraction synthesis. *Computer Graphics Forum*, 37(4):167–176, 2018. doi: 10.1111/cgf.13484

[34] R. Shapley and C. Enroth-Cugell. Visual adaptation and retinal gain controls. *Progress in retinal research*, 3:263–346, 1984.

[35] S. Soon, A. Lugmayr, A. Woods, and T. Tan. Understanding head-mounted display fov in maritime search and rescue object detection. In *Proceedings - 2018 IEEE International Conference on Artificial Intelligence and Virtual Reality, AIVR 2018*, pp. 116–119. Institute of Electrical and Electronics Engineers Inc., 1 2019. doi: 10.1109/AIVR.2018.00023

[36] L. Spadea, G. Maraone, F. Verboschi, E. M. Vingolo, and D. Tognetto. Effect of corneal light scatter on vision: a review of the literature. *International journal of ophthalmology*, 9(3):459, 2016.

[37] V. V. Tuchin. Light scattering study of tissues. *Physics-Uspekhi*, 40(5):495–515, 5 1997. doi: 10.1070/pu1997v040n05abeh000236

[38] T. J. T. P. Van Den Berg. Importance of pathological intraocular light scatter for visual disability. *Documenta Ophthalmologica*, 61(3-4):327–333, 1 1986. doi: 10.1007/BF00142360

[39] T. J. T. P. van den Berg, M. P. J. Hagenouw, and J. E. Coppens. The ciliary corona: Physical model and simulation of the fine needles radiating from point light sources. *Investigative Ophthalmology & Visual Science*, 46(7):2627–2632, 1 2005. doi: 10.1167/iovs.04-0935

[40] T. J. T. P. van den Berg and H. Spekreijse. Light scattering model for donor lenses as a function of depth. *Vision Research*, 39(8):1437–1445, 1999. doi: 10.1016/S0042-6989(98)00220-X

[41] P. Vangorp, K. Myszkowski, E. W. Graf, and R. K. Mantiuk. A model of local adaptation. *ACM Trans. Graph.*, 34(6):166:1–166:13, 10 2015. doi: 10.1145/2816795.2818086

[42] N. J. Volpe. Adler's physiology of the eye: Clinical application, tenth edition. *Journal of Neuro-Ophthalmology*, 24(4), 2004.

[43] J. Wienold and J. Christoffersen. Evaluation methods and development of a new glare prediction model for daylight environments with the use of ccd cameras. *Energy and buildings*, 38(7):743–757, 2006.

[44] C. Wyman, P.-P. Sloan, and P. Shirley. Simple analytic approximations to the cie xyz color matching functions. Technical Report 2, NVIDIA, 2013.

[45] A. Yoshida, V. Blanz, K. Myszkowski, and H.-P. Seidel. Perceptual evaluation of tone mapping operators with real-world scenes. In B. E. Rogowitz, T. N. Pappas, and S. J. Daly, eds., *Human Vision and Electronic Imaging X*, vol. 5666, p. 192 – 203. SPIE, 2005. doi: 10.1117/12.587782

[46] A. Yoshida, M. Ihrke, R. Mantiuk, and H.-P. Seidel. Brightness of the glare illusion. In *Proceedings of the 5th Symposium on Applied Perception in Graphics and Visualization*, APGV '08, pp. 83–90. ACM, New York, NY, USA, 2008. doi: 10.1145/1394281.1394297

[47] J. F. Zapata-Díaz, H. Radhakrishnan, W. N. Charman, and N. López-Gil. Accommodation and age-dependent eye model based on in vivo measurements. *Journal of Optometry*, 12(1):3–13, 2019. doi: 10.1016/j.optom.2018.01.003